Proc. Natl. Acad. Sci. USA
Vol. 91, pp. 10370–10374, October 1994
Immunology

Conformational isomerism and the diversity of antibodies

JEFFERSON FOOTE† AND CÉSAR MILSTEIN‡

†Fred Hutchinson Cancer Research Center, 1124 Columbia Street C3-168, Seattle, WA 98104; and ‡Medical Research Council Laboratory of Molecular Biology, Hills Road, Cambridge, CB2 2QH, England

Contributed by César Milstein, June 24, 1994

ABSTRACT **The fact that one cell encodes a single antibody sequence does not necessarily mean that the resulting antibody folds into a single structure, although this is a common assumption. Here we challenge this view and suggest that many antibodies do not have a single conformation at the combining site. The basis for this proposal comes from the kinetic analysis of a set of murine hybridomas derived from defined stages of the immune response to 2-phenyl-5-oxazolone (Ox). Among them we have identified three antibodies that exhibit complex hapten-binding kinetics. We observed biphasic or triphasic reactions in stopped-flow fluorescence experiments, indicating that ligand binding involved isomerization, as well as associative steps. The existence of an equilibrium between at least two antibody conformations, with ligands binding preferentially to one form, was deduced from the variation with hapten concentration of the apparent rate of each phase.**

Since Clonal Selection replaced the Instructive Theory as a working model of immunity, the axiom of one-lymphocyte-one-antibody has been equated to one combining site (1–4). Experiments defining the basis of humoral immune diversity have emphasized combinatorial and somatic mutational processes that lead to covalent diversity of the antibody repertoire (5). Nevertheless, two independent lines of evidence exist for diversity at the level of antibody tertiary structure. Certain crystal structures of antibodies with and without ligands have shown conformation dimorphism, which could only partly be attributed to crystallization artifacts (6–8). Despite the rich detail of these structures, crystallographically detected conformational differences due to ligation are mechanistically ambiguous (9). Differences could arise from direct interaction with the ligand (induced fit) or, with equal plausibility, by preferential ligand binding to a preexisting subpopulation of antibody isomers. This distinction is of considerable immunological consequence, since two isomers in spontaneous equilibrium would both form part of the humoral repertoire, whereas an induced conformation existing only in an immune complex would not contribute to diversity in the same way. Kinetic analysis avoids this particular ambiguity. Indeed, studies on several myeloma proteins have demonstrated kinetically distinct conformational isomers (10–13). It could be argued that myeloma cells have an uncertain ontogeny and are not subject to the immune maturation mechanisms encountered in a bona fide antigenic response; however, similar kinetic behavior was reported for an anti-fluorescein hybridoma (14). Some of these cases demonstrate a preexisting isomeric equilibrium and others are consistent with an induced-fit mechanism. Notwithstanding this evidence that conformational polymorphism can occur, the isolated examples uncovered through either structural or kinetic approaches leave an uncertainty whether antibody isomerism is an oddity or a general and important factor in an immune response.

The publication costs of this article were defrayed in part by page charge payment. This article must therefore be hereby marked "*advertisement*" in accordance with 18 U.S.C. §1734 solely to indicate this fact.

Here we address the lack of a context for evaluating the role of isomerism in monoclonal antibodies from hybridomas derived from an immune response. The humoral response to the hapten 2-phenyl-5-oxazolone (Ox) in BALB/c mice is highly reproducible, inasmuch as use of the same canonical variable region (V) genes has been observed repeatedly, often with identical somatic point mutations. Previous reports from our laboratory have described derivation and antibody mRNA sequence analysis of a large number of hybridomas from discrete stages of the Ox response (15–20). We have also presented an analysis of the hapten-binding kinetics of 40 monoclonal antibodies from this collection (21). Most of these reactions followed simple first-order kinetics, but three appeared more complex, suggesting the occurrence of an isomerization. Thus some form of conformational diversity was potentially manifest within the context of an extremely well-characterized immune response. Here we report mechanistic analysis of these three molecules and the implication of their shared features.

MATERIALS AND METHODS

Antibodies and Haptens. Hybridoma lines NQ10/4.6.2, NQ22/33.4, and NQ22/61.1 have been characterized previously (17, 18). Antibodies from these cell lines were all IgG1,κ type, and they were purified by affinity chromatography on staphylococcal protein A-Sepharose. Ox-aminocaproate (Ox-cap) was synthesized by a published method (22). Ox-iminodiacetate (Ox-IDA) and amino-Ox (Ox-NH_2) were synthesized by using analogous procedures, by addition of ethanolic ethoxymethylene-Ox to aqueous iminodiacetate or NH_4HCO_3. Crude Ox-IDA was recrystallized from acetone/H_2O and dimethylformamide/H_2O. An Ox-NH_2 stock solution was made in ethanol and diluted into aqueous buffer just before use. Although the solubility of Ox-NH_2 in the reaction buffer is 13 μM, slightly supersaturated solutions prepared in this manner were stable for the duration of a kinetic experiment.

Stopped-Flow Methods. Kinetic measurements were made with a Hi-Tech Scientific stopped-flow fluorescence instrument (21). Antibody at a site-basis concentration of 125–250 nM was allowed to react with hapten that at equilibrium was in at least 10-fold excess. Reactions were buffered at pH 7, 20°C in 25 mM NaH_2PO_4/125 mM NaCl/0.1 mM EDTA. To detect the quenching of native antibody fluorescence, excitation was at 280 nm, and emission was monitored through a 320-nm cutoff filter.

Primary Data Analysis. Transients from 15–75 reactions were averaged to improve the signal-to-noise ratio. Averaged data were fit to an exponential, using software provided by the stopped-flow manufacturer, although for the antibodies in this study, systematic deviations from the fitted curve were

Abbreviations: Ox, 2-phenyl-5-oxazolone; Ox-cap (Ox-aminocaproate), 2-phenyl-4-carboxybutylaminomethylene-5-oxazolone; Ox-IDA (Ox-iminodiacetate), 2-phenyl-4-bis(carboxymethyl)-iminomethylene-5-oxazolone; Ox-NH_2 (amino-Ox), 2-phenyl-4-aminomethylene-5-oxazolone; V, variable region; Ab, antibody; L, ligand.

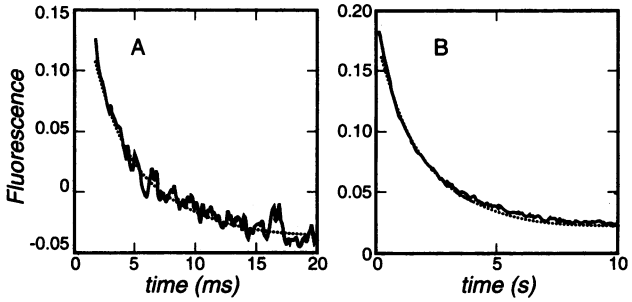

FIG. 1. Complex kinetics in the reaction of anti-Ox antibody NQ22/61.1 with the hapten Ox-IDA. (*A*) Initial phase. (*B*) Subsequent phase. Dotted lines represent an attempted least-squares fit to a single exponential. Because of instrumental constraints on data collection, separate reactions were used for the very rapid first phase and the slower biphasic process observed subsequently. The lack of correspondence between the terminal fluorescence of the curve in *A* and the initial fluorescence of the curve in *B* reflects separate adjustment of the instrument gain for each reaction, to achieve the highest sensitivity.

generally observed. Consequently, data were fit to a double exponential, again using the manufacturer's software. In the case of the triphasic kinetics of antibody NQ22/61.1, the fast phase was sufficiently resolved that the system could be treated as a combination of a single exponential and double exponential. Each fit thus provided one to three apparent rate constants with standard errors.

Secondary Data Analysis. The apparent rate constants extracted from fits of the primary data generally do not reflect discrete chemical steps, and we designate these empirically as k_{fast}, k_{medium}, and k_{slow}. Instead, these parameters are functions of a combination of terms, including ligand concentration and true rate constants for individual steps, which we denote with k_1, k_2, etc. To analyze triphasic reactions, we sorted the apparent rate constants into fast, medium, and slow sets. The three sets were fit simultaneously by least squares (23) to the corresponding expressions for r, the variable for empirical rate constants described below in Eqs. 9, to optimize a common set of true kinetic constants. Because of the extended range in rates, a logarithmic fit was used—i.e., the quantity minimized was $(\log r_{observed} - \log r_{calculated})^2$.

RESULTS

Triphasic Kinetics with Antibody NQ22/61.1. The reaction of Ox-IDA with antibody NQ22/61.1, measured by quenching of antibody fluorescence in a stopped-flow instrument, is shown in Fig. 1. One phase of the reaction appears to be complete within 20 ms (Fig. 1*A*). However, the reaction continues over the following 10 s (Fig. 1*B*). This subsequent process is in turn biphasic; attempts to fit later data points to a simple exponential invariably gave systematic deviations in the residuals. Thus the reaction of NQ22/61.1 followed overall triphasic kinetics.

In the initial discovery of antibody isomerism (10), myeloma protein MOPC 460 showed a biphasic interaction with low-affinity ligands, leading to proposal of the following mechanism:

$$\begin{array}{ccc} L + Ab & \underset{k_{-4}}{\overset{k_4}{\rightleftharpoons}} & AbL \\ k_1 \downarrow\uparrow k_{-1} & & k_3 \downarrow\uparrow k_{-3} \\ L + Ab^* & \underset{k_{-2}}{\overset{k_2}{\rightleftharpoons}} & Ab^*L \end{array}$$

Mechanism I

In this model, an antibody exists in an equilibrium between two conformations, Ab and Ab*. Differential reactivity of the two isomers toward ligand (L) gives rise to complex kinetics, which according to relaxation theory (10, 24) should be triphasic. To our knowledge, no triphasic antibody–hapten reaction has previously been reported. The absence of a third phase in earlier studies (10–14) has been attributed variously to experimental difficulties in detecting very short relaxation times or low amplitudes, or to the system approximating a limiting case of Mechanism I. The operation of Mechanism I in these cases was inferred from quantitative incongruities in other parameters, such as independently measured equilibrium constants or relaxation amplitudes.

Kinetic Theory of Mechanism I. Our stopped-flow experiments initiate from separate reactants, rather than from a point near equilibrium, hence relaxation theory (10, 24) is not strictly applicable. Here we present a different treatment, which employs the approximation that the concentration of a ligand present in great excess is effectively constant over the course of a reaction, but which otherwise is exact. Mechanism I can be described by a system of four linear homogeneous first-order differential equations:

$$d[Ab]/dt = -(k_1 + k_4[L])[Ab] + k_{-1}[Ab^*] + k_{-4}[ABL], \quad [1]$$

$$d[Ab^*]/dt = k_1[Ab] - (k_{-1} + k_2[L])[Ab^*] + k_{-2}[Ab^*L], \quad [2]$$

$$d[Ab^*L]/dt = k_2[L][Ab^*] - (k_{-2} + k_{-3})[Ab^*L] + k_3[AbL], \quad [3]$$

$$d[AbL]dt = k_4[L][Ab] + k_{-3}[Ab^*L] - (k_{-4} + k_3)[AbL]. \quad [4]$$

When this system is solved by matrix methods, three nonzero eigenvalues arise, again leading to prediction of a triphasic reaction. At a given ligand concentration, L, these are equal to the three roots, r, of the cubic equation

$$\begin{aligned} &r^3 + r^2(k_1 + k_{-1} + k_2L + k_{-2} + k_3 + k_{-3} + k_4L + k_{-4}) \\ &+ r(k_{-1}k_4L + k_1k_2L + k_2k_4L^2 + k_{-2}k_{-4} + k_{-3}k_{-4} + k_{-2}k_3 \\ &+ k_{-1}k_{-4} + k_2k_{-4}L + k_1k_{-4} + k_{-1}k_3 + k_2k_3L + k_1k_3 + k_3k_4L \\ &+ k_{-1}k_{-2} + k_1k_{-2} + k_{-2}k_4L + k_{-1}k_{-3} + k_2k_{-3}L + k_1k_{-3} \\ &+ k_{-3}k_4L) + k_1k_2k_{-4}L + k_{-1}k_3k_4L + k_1k_2k_3L + k_2k_3k_4L^2 \\ &+ k_{-1}k_{-2}k_4L + k_{-1}k_{-3}k_4L + k_1k_2k_{-3}L + k_2k_{-3}k_4L^2 \\ &+ k_{-1}k_{-2}k_{-4} + k_{-1}k_{-3}k_{-4} + k_{-1}k_{-2}k_3 + k_2k_{-3}k_{-4}L \\ &+ k_1k_{-2}k_{-4} + k_1k_{-3}k_{-4} + k_1k_{-2}k_3 + k_{-2}k_3k_4L = 0. \end{aligned} \quad [5]$$

To calculate the cubic roots (25) we assign simplifying coefficients of the form

$$r^3 + a_1r^2 + a_2r + a_3 = 0 \quad [6]$$

and substitute

$$Q = \{a_1^2 - 3a_2\}^{1/2}/3 \quad [7]$$

and

$$\theta = \arccos \frac{2a_1^3 - 9a_1a_2 + 27a_3}{54Q^3}. \quad [8]$$

The three values of r, corresponding to the three apparent rate constants constituent to a triphasic reaction, can then be calculated from

$$r = -2Q\cos(\phi/3) - a_1/3 \quad \text{for} \quad \phi = \theta, \theta + 2\pi, \theta + 4\pi. \quad [9]$$

The fluorescence change as a function of time is then given by

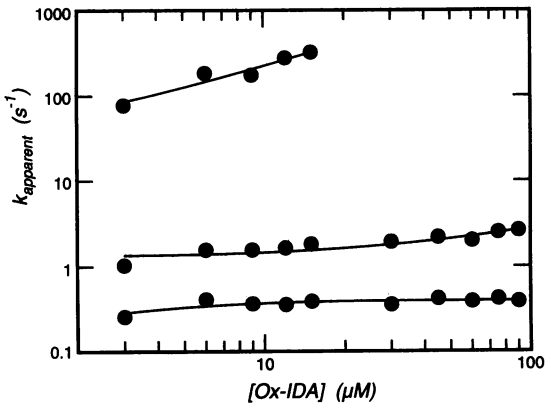

FIG. 2. Behavior of the three phases of the reaction of NQ22/61.1 with Ox-IDA. The fast phase of the reaction was observed on a short time scale and was fit to a single exponential. Values of the fast apparent rate constant, obtained from such fits, form the top group of points. Data for the two slower phases were obtained in a separate experiment, from a fit to a double exponential, and they form the middle and bottom groups of points. Theoretical lines calculated from least-squares fits of the data to Eqs. 9 connect the points.

$$F(t) = F_1\exp(-r_\theta t) + F_2\exp(-r_{\theta+2\pi} t) + F_3\exp(-r_{\theta+4\pi} t). \quad [10]$$

Here, the amplitudes F_1, F_2, and F_3 are measured experimentally, but they cannot be derived without assumptions of the fluorescence quantum yield of the individual steps in Mechanism I.

Consistency of NQ22/61.1 with Mechanism I. To determine whether NQ22/61.1 could follow this model, we measured kinetics of reaction with Ox-IDA over a range of hapten concentrations. The apparent rate constants of the three phases are plotted in Fig. 2. We fit data points to the expressions in Eqs. 9 by least squares to obtain values for the rate constants of the individual steps of Mechanism I. Standard errors of the forward rate constants, k_1, k_2, k_3, and k_4, were all <25%. Great imprecision was found in the reverse rate constants, however; hence meaningful equilibrium constants for the different steps could not be calculated. Nevertheless, theoretical lines based on fitted parameters conform closely to the experimental points, as can be seen in Fig. 2. Thus Mechanism I is the simplest chemical model consistent with the complex kinetic behavior of NQ22/61.1.

Biphasic Kinetics with Antibodies NQ22/33.4 and NQ10/4.6.2. We observed biphasic reactions of Ox haptens with antibodies NQ22/33.4 and NQ10/4.6.2. This could signify a failure to detect an existing third phase or operation of a simpler binding mechanism. We first consider the latter possibility. Two kinetic mechanisms that comprise a single association step and a single isomerization in consecutive order predict biphasic kinetics (26):

$$\mathrm{Ab} + \mathrm{L} \underset{k_{-1}}{\overset{k_1}{\rightleftarrows}} \mathrm{AbL} \underset{k_{-2}}{\overset{k_2}{\rightleftarrows}} \mathrm{Ab^*L}$$

Mechanism II

$$\mathrm{Ab} \underset{k_{-1}}{\overset{k_1}{\rightleftarrows}} \mathrm{Ab^*} + \mathrm{L} \underset{k_{-2}}{\overset{k_2}{\rightleftarrows}} \mathrm{Ab^*L}$$

Mechanism III

Mechanism II is an induced-fit model. Here the initial hapten–antibody interaction causes changes in either or both reactants, leading to an improved binding geometry, with possible changes in fluorescence quantum yield. In Mechanism III, an equilibrium preexists between two antibody conformations, only one of which is capable of binding antigen. The fast reaction phase would approximate a burst of binding to the active conformation in this mechanism, and the slow phase a further combination with hapten, occurring as the isomeric antibody species reequilibrate. The two mechanisms represent limiting cases of Mechanism I, with Mechanism II equivalent to the clockwise arm of the Ab to Ab*L pathway, the Mechanism III the counterclockwise arm.

The apparent rate constants, k_{slow} and k_{fast}, for the two phases of Mechanisms II and III again correspond to combinations of true rate constants for individual steps. The two mechanisms may be distinguished by the behavior of k_{slow} as ligand concentration is varied. Mechanism II predicts a rise in k_{slow} with increasing ligand, up to a plateau value, whereas Mechanism III predicts a decrease to a limiting value. Only linear behavior was observed with the high-affinity ligand Ox-cap (not shown). However, kinetic equations (26) predict that the change in k_{slow} for either mechanism is negligible at saturating ligand but is most pronounced at ligand concentrations below the equilibrium dissociation constant, K_d. Consequently, we synthesized weaker-affinity haptens to facilitate experimental determination of the respective kinetic mechanisms of NQ22/33.4 and NQ10/4.6.2. These molecules retained the main recognition elements of the phenyloxazolone moiety but had amino (Ox-NH_2) or iminodiacetate (Ox-IDA) groups in place of the exocyclic lysine-like substituent common to high-affinity ligands. Antibody NQ22/33.4 bound Ox-IDA with a K_d of 4.3 μM. Reaction of NQ22/33.4 with Ox-IDA showed the progressive decrease in k_{slow} (Fig. 3*A*) characteristic of the preexisting equilibrium model of Mechanism III. Antibody NQ10/4.6.2 did not bind Ox-IDA, but it bound Ox-NH_2 with a K_d of 9 μM. NQ10/4.6.2 also showed kinetic behavior of k_{slow} (Fig. 3*B*) consistent with Mechanism III. Thus, the experiments in Fig. 3 rule out an induced-fit mechanism for hapten binding by NQ22/33.4 and NQ10/4.6.2 and demonstrate the existence of an equilibrium between isomeric forms of the two antibodies.

Forced Binding at High Hapten Concentration. Mechanism III quantitatively accounts for the binding kinetics observed at low hapten concentrations. However, Mechanism III is too

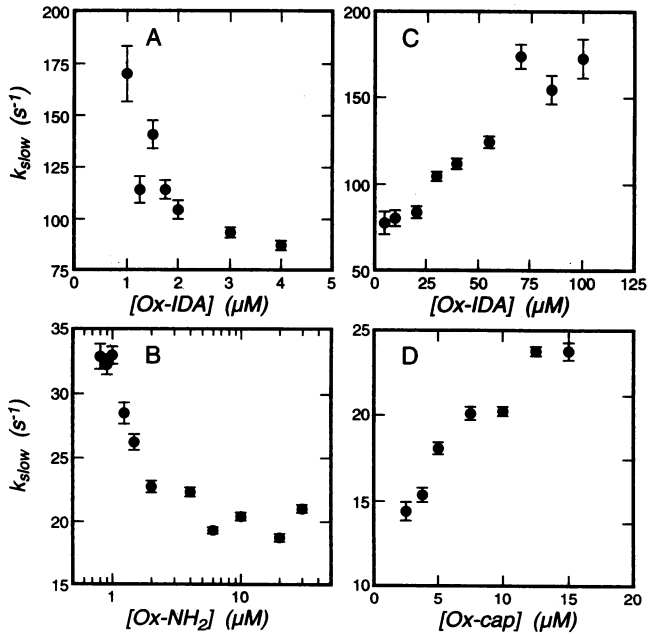

FIG. 3. Concentration dependence of the slow phase of biphasic reactions. (*A* and *C*) Reaction of antibody NQ22/33.4 with Ox-IDA. (*B*) Reaction of NQ10/4.6.2 with Ox-NH_2. (*D*) Reaction of NQ10/4.6.2 with Ox-cap.

simple, because k_{slow} does not reach a limiting value, but rises at hapten concentrations high relative to K_d. Thus reactions of NQ22/33.4 with high concentrations of Ox-IDA show an increase in k_{slow} with ligand concentration above 5 μM (Fig. 3*C*). A similar experiment with NQ10/4.6.2 binding the high-affinity hapten Ox-cap (Fig. 3*D*) also showed k_{slow} increasing with ligand concentration. (Studies at high concentrations of Ox-NH_2 were not possible due to low solubility.) These results are incompatible with Mechanism III, but they can be explained by Mechanism I. While it could be argued that an "induced-fit" component is needed to complete the kinetic data, this is quantitatively meaningful at concentrations of antigen which are rather high and unlikely to be important during immunization. A better explanation is that the species Ab is not inert, but retains some residual affinity for Ox, and binding to Ab becomes measurable at high ligand concentration. This weak-affinity pathway would form the clockwise route between Ab and Ab*L in Mechanism III. While the kinetics of this system is formally triphasic, the two slower rate processes would dominate the fluorescence change of the reaction at opposite ends of the ligand concentration range, together giving the experimental appearance of a single exponential and overall biphasic kinetics. Numerical analysis supports this interpretation. Data points from the slow phase of NQ22/33.4 were separated into high-hapten and low-hapten ranges. The two groups were assigned to independent rate processes, then with the third group of k_{fast} values, were fit to the three equations of Mechanism I. Kinetic constants obtained from the least-squares solution were used to calculate theoretical lines, which closely approximated the experimental points (not shown). A similar treatment was not possible for NQ10/4.6.2, since a different hapten was necessary for the high concentration range.

Elimination of Trivial Explanations. Complex kinetics could be trivial. Contamination of cell lines or loss of clonality resulting from *"in vitro"* mutations, yielding antibody preparations containing two or three molecular species reacting at very different rates, could give rise to multiphasic kinetics such as those shown in Fig. 1. However, the rate of independent associative reactions should increase linearly with hapten concentration, whereas the slow phases of the observed reactions (Figs. 2 and 3) tended to remain constant or decrease in rate with increasing hapten. A second possible origin of complex kinetics is the ligand-induced dissociation of antibody aggregates. We tested this possibility in a sedimentation velocity experiment. Antibody NQ22/33.4 sedimented in the absence and presence of saturating Ox-cap with $s_{20,w}$ values of 6.8 and 6.9 S, respectively, ruling out changes in quaternary structure (data contributed by Y. Yang and H. K. Schachman). A third potential artifact could come from the rotational isomerization of the side chain about the exocyclic C—N bond in the oxazolone, known from NMR data to occur on a 0.1–1 s^{-1} time scale (27). However, reactions of the antibodies with Ox derivatives with symmetrical amino or iminodiacetate side chains still showed multiphasic kinetics (Figs. 1–3), eliminating this possibility. Thus the complex kinetics of these antibodies appears intrinsic to antigen recognition.

DISCUSSION

Our kinetic analysis demonstrates that the three Ox antibodies studied all exist in an equilibrium between isomeric states. The data do not allow us an accurate estimation of the molar ratios of both isomers. However, the roughly equivalent fluorescence amplitudes of the fast and slow phases indicate that a substantial proportion of each species makes up this equilibrium in the absence of antigen. Although Mechanism I formally includes an induced-fit component, NQ22/33.4 and NQ10/4.6.2 approach a limiting case of this mechanism, in which this component is negligible, while high-affinity binding to Ab* represents the major pathway of antigen recognition. That these observations arise in the context of an immune response whose repertoire evolution has been extensively mapped at the sequence level enables us to add two conclusions that could not be drawn from earlier kinetic and crystallographic studies. First, antibody isomerism is not rare: our three examples are from a total of just 40 Ox-specific hybridomas. Furthermore, these three antibodies use distinct combinations of light and heavy chain V-gene families. NQ10/4.6.2 (Vκ45 and M21), NQ22/33.4 (Vκ45 and group 6), and NQ22/61.1 (Ox1 and M21), showed different pairings, thus the three molecules in this study are distinct structures of independent origin. By contrast, many of the remaining antibodies are iterations of the canonical anti-Ox genes, V_H-Ox1 and V_κ-Ox1. Given the multiplicity of occurrence and the improbability that the anti-Ox response represents a special case, it may be valid to extrapolate that a tenth of *all* antibodies show this form of isomerism. However, isomerism may be more general. The phenomenon cannot be detected by equilibrium techniques, nor do kinetic techniques guarantee detection of isomeric equilibria, as the magnitude of rate constants or amplitudes could easily give the appearance of a simple binding mechanism. Thus isomerism detected by kinetic data may represent only the tip of an iceberg.

We conclude, second, that, rather than being eliminated during immune maturation, lymphocytes expressing isomeric antibodies compete effectively with other lymphocytes, even in hyperimmune responses. One antibody (NQ10/4.6.2) originates from the secondary immune response, and the other two from the tertiary. Sequence data show that each has undergone somatic mutation. The V_κ-Ox1-derived light chain of NQ22/61.1, for example, has seven protein-coding mutations relative to the germ-line sequence, including characteristic mutations at residues 34 and 36. Mutations at these sites are found in nearly all Ox-specific V_κ-Ox1 derivatives, and the side chains at these positions have been shown in a crystal structure to interact directly with hapten (28). The hapten affinities of the three isomeric molecules show between 3- and 18-fold-enhanced hapten affinity compared with the unmutated canonical Ox antibody (17, 18, 21). Such increases are not particularly high for the secondary and tertiary responses, but this in part may be attributed to the energetic cost of isomerization. Furthermore, the antibody with the weakest affinity, NQ22/61.1, shows a very high hapten association rate constant (on-rate) for one of its isomers; we have argued previously that a fast on-rate is a physical property of significant selective value during immune maturation (21).

Structural differences distinguishing the anti-Ox conformations, whatever they may be, clearly are sufficient that only one isomer binds a specific antigen well. However, an inactive isomer could in principle be the preferred receptor for a second antigen of substantially different structure. The implication for immune diversity of antibodies with potential multiple antigen specificity due to conformational isomers is that the number of lymphocytes in an animal does not limit the available repertoire.

The existence of a combining site in multiple conformations invites several predictions. First, antibodies in the primary repertoire may be more prone to isomerism. Indeed, evolution may favor V genes likely to display such behavior to increase diversity. Second, while we consider only isomerism between two configurations, a more complex picture is likely in at least some examples. Third, isomers which occur in approximately equal molar ratios are easier to detect but not likely to represent the most common pattern. However, a very disfavorable isomeric equilibrium, which will decrease the effective affinity, may still allow B-cell proliferation.

Affinity maturation in such cases may include mutations leading to a more favorable isomeric equilibrium. Indeed, we cannot exclude the possibility that the mature antibodies described in this paper did not originate from primary antibodies with a much less favorable equilibrium. Fourth, mutations responsible for such alterations in the isomeric equilibrium could increase affinity without modification of the combining site itself. Fifth, isomerism could potentiate a type of cross-reactivity in which an antibody conformational change mediates recognition of dissimilar antigens, in effect yielding a bispecific antibody.

We thank J. M. Jarvis for contributing purified protein and sequencing data, R. Hawkins for checking the kinetic equations, and Y. R. Yang and H. K. Schachman for performing the ultracentrifugation experiment. In addition, we thank G. Winter and R. Hawkins for reading the manuscript. This work was performed at the Medical Research Council Laboratory of Molecular Biology, where J.F. was supported by a Merck Fellowship.

1. Burnet, F. M. (1959) *The Clonal Selection Theory of Acquired Immunity* (Vanderbilt Univ. Press, Nashville, TN), pp. 53–61.
2. Talmage, D. W. (1959) *Science* **129,** 1643–1648.
3. Lederberg, J. (1959) *Science* **129,** 1649–1653.
4. Pauling, L. (1940) *J. Am. Chem. Soc.* **62,** 2643–2653.
5. Tonegawa, S. (1983) *Nature (London)* **302,** 575–581.
6. Herron, J. N., He, X. M., Ballard, D. W., Blier, P. R., Pace, P. E., Bothwell, A. L., Voss, E. W., Jr., & Edmundson, A. B. (1991) *Proteins Struct., Function Genet.* **11,** 159–175.
7. Rini, J., Schulze-Gamen, U. & Wilson, I. A. (1992) *Science* **255,** 959–965.
8. Bhat, T. N., Bentley, G. A., Fischmann, T. O., Boulot, G. & Poljak, R. J. (1990) *Nature (London)* **347,** 483–485.
9. Stevens, F. J., Chang, C.-H. & Schiffer, M. (1988) *Proc. Natl. Acad. Sci. USA* **85,** 6895–6899.
10. Lancet, D. & Pecht, I. (1976) *Proc. Natl. Acad. Sci. USA* **73,** 3548–3553.
11. Vuk-Pavlovic, S., Blatt, Y., Glaudemans, C. P., Lancet, D. & Pecht, I. (1978) *Biophys. J.* **24,** 161–174.
12. Zidovetski, R., Blatt, Y., Glaudemans, C. P., Manjula, B. N. & Pecht, I. (1980) *Biochemistry* **19,** 2790–2795.
13. Pecht, I. (1982) in *The Antigens*, ed. Sela, M. (Academic, New York), Vol. 6, pp. 1–68.
14. Kranz, D. M., Herron, J. N. & Voss, E. W. (1982) *J. Biol. Chem.* **257,** 6987–6995.
15. Kaartinen, M., Griffiths, G. M., Markham, A. F. & Milstein, C. (1983) *Nature (London)* **304,** 320–324.
16. Griffiths, G. M., Berek, C., Kaartinen, M. & Milstein, C. (1984) *Nature (London)* **312,** 271–275.
17. Berek, C., Griffiths, G. M. & Milstein, C. (1985) *Nature (London)* **316,** 412–418.
18. Berek, C., Jarvis, J. M. & Milstein, C. (1987) *Eur. J. Immunol.* **17,** 1121–1129.
19. Berek, C. & Milstein, C. (1987) *Immunol. Rev.* **96,** 23–41.
20. Berek, C. & Milstein, C. (1988) *Immunol. Rev.* **105,** 5–26.
21. Foote, J. & Milstein, C. (1991) *Nature (London)* **352,** 530–532.
22. Mäkelä, O., Kaartinen, M., Pelkonen, J. L. T. & Karjalainen, K. (1978) *J. Exp. Med.* **148,** 1644–1660.
23. Marquardt, D. W. (1963) *J. Soc. Ind. Appl. Math.* **11,** 431–441.
24. Castellan, G. W. (1963) *Ber. Bunsenges. Phys. Chem.* **67,** 898–908.
25. Press, W. H., Flannery, B. P., Teukolsky, S. A. & Vetterling, W. T. (1989) *Numerical Recipes in Pascal* (Cambridge Univ. Press, Cambridge, U.K.), pp. 164–165.
26. Fersht, A. (1977) *Enzyme Structure and Mechanism* (Freeman, New York), pp. 118–121.
27. Titman, J. J., Foote, J., Jarvis, J. M., Keeler, J. & Neuhaus, D. (1991) *Chem. Commun.*, 419–421.
28. Alzari, P. M., Spinelli, S., Mariuzza, R. A., Boulot, G., Poljak, R. J., Jarvis, J. M. & Milstein, C. (1990) *EMBO J.* **9,** 3807–3814.